

# *XMM-Newton* and Canadian Galactic Plane Survey Observations of the Supernova Remnant G107.5–1.5

M. S. Jackson<sup>1 2 3\*</sup>, S. Safi-Harb<sup>1 4</sup>, & R. Kothes<sup>5</sup>

<sup>1</sup>*Department of Physics and Astronomy, University of Manitoba, Winnipeg, MB, R3T 2N2, Canada*

<sup>2</sup>*Department of Physics, KTH Royal Institute of Technology, Stockholm, Sweden*

<sup>3</sup>*The Oskar Klein Centre for Cosmoparticle Physics, AlbaNova University Centre, Stockholm, Sweden*

<sup>4</sup>*Canada Research Chair*

<sup>5</sup>*Dominion Radio Astrophysical Observatory, National Research Council Herzberg, P.O. Box 248, Penticton, BC, V2A 6J9, Canada*

Accepted . Received ; in original form 2013 July 19

## ABSTRACT

We present an *XMM-Newton* observation of the highly polarized low-surface brightness supernova remnant G107.5–1.5, discovered with the Canadian Galactic Plane Survey (CGPS). We do not detect diffuse X-ray emission from the SNR and set an upper limit on the surface brightness of  $\sim 2 \times 10^{30}$  erg arcmin<sup>-2</sup> s<sup>-1</sup>, at an assumed distance of 1.1 kpc. We found eight bright point sources in the field, including the *ROSAT* source 1RXS J225203.8+574249 near the centre of the radio shell. Spectroscopic analysis of some of the embedded point sources, including the *ROSAT* source, has been performed, and all eight sources are most likely ruled out as the associated neutron star, primarily due to counterpart bright stars in optical and infrared bands. Timing analysis of the bright point sources yielded no significant evidence for pulsations, but, due to the timing resolution, only a small part of the frequency space could be searched. An additional ten fainter point sources were identified in the vicinity of the SNR. Further X-ray observation of these and the region in the vicinity of the radio shell may be warranted.

**Key words:** ISM: supernova remnant. ISM: individual object: G107.5–1.5. stars: neutron. X-rays: ISM. polarization: supernova remnants

## 1 INTRODUCTION

Low-surface brightness supernova remnants (SNRs) are important in shaping our current understanding of pulsar and supernova evolution, since the population of SNRs in our Galaxy is likely to be dominated by faint objects. In fact, around 85% of Galactic SNRs are expected to be of core-collapse origin (Tsujimoto et al. 1995). These are explosions of massive stars, most of which create stellar wind bubbles around them, and thus form low-surface brightness SNRs. Massive star explosions should also lead to the formation of a compact object that could be revealed in the radio and/or X-rays. High-resolution *Chandra* and *XMM-Newton* observations have been particularly crucial in shedding light on the collapsed cores of the explosions and their relativistic outflows (see Kargaltsev & Pavlov 2008; Vink 2012).

In particular, high-resolution and sensitive X-ray observations have contributed to the discovery of a diversity of neutron stars in SNRs. This diversity includes rotation-powered pulsars such as the Crab and Vela pulsars, magnet-

ically powered pulsars (dubbed as ‘magnetars’ and including the Anomalous X-ray Pulsars and Soft Gamma-ray Repeaters), and other X-ray emitting neutron stars whose nature is still being debated (see e.g. Mereghetti 2012). These include the Central Compact Objects (CCOs) in SNRs and are typified by the CasA compact object (e.g. Gotthelf & Halpern 2008). Finding new compact objects in SNRs will therefore help in shedding light on this diversity and on the connection between the compact objects and the progenitor stars forming their hosting SNR.

The Canadian Galactic Plane Survey (CGPS) (Taylor et al. 2003) is a high-resolution radio survey that incorporates single-antenna data to retain sensitivity to the largest structures (such as faint filamentary non-thermal radio emission from SNRs). In 2001, the shell-type supernova remnant (SNR), G107.5–1.5, was discovered in CGPS data (Kothes 2003). Including the one described in this paper, eight SNR candidates have so far been discovered in the CGPS (Kothes et al. 2001, 2005; Tian, Leahy, & Foster 2007; Foster et al. 2013). In 2008, we started a program to search for these SNRs and their associated compact objects in *Chandra* and

\* E-mail: mirandaj@kth.se

*XMM-Newton* data (see e.g. Jackson, Safi-Harb, Kothes, & Foster 2008).

The SNR G107.5–1.5 is located in a complex region of the Galactic plane  $\sim 4$  degrees west of Cas A (Kothes 2003). At 1420 MHz, the source appears as a thin filament on top of diffuse shell-like emission (see contours in Figure 1). Combining the 408 MHz and the 1420 MHz emission, the spectral index was determined to be  $\alpha \sim 0.6$  ( $S_\nu \propto \nu^{-\alpha}$ ) – typical of shell-type SNRs. Its identification as an SNR is based mainly on its high polarized emission coincident with the filament and spectral index. Its polarized intensity is 50% at 1420 MHz, and its peak fractional polarization of 71% is close to the theoretical maximum (for  $\alpha=0.6$ ). This was therefore identified as the most highly polarized SNR known. The distance to this SNR from various distance determination methods (as described in Kothes 2003) is  $1.1 \pm 0.4$  kpc. The morphology of the SNR and the structure of the ambient neutral hydrogen in the radio data suggests that this SNR is  $\sim 3$ –6 kyr-old, and believed to be in a late stage of evolution, given that it is expanding in a high ambient density medium or originates from a supernova with low explosion energy (Kothes 2003).

At the projected centre of the SNR shell, there is a *ROSAT* unidentified source, 1RXS J225203.8+574249, whose location is quite compelling: not only is it close to the projected centre of the SNR, but if it is a neutron star and the explosion happened at its current position, then it would explain the peculiar appearance of the SNR as a shell fragment. In all directions, the wind of the progenitor and the shock wave of the explosion would have been blocked by dense neutral hydrogen except for the gap in the direction of the radio shell. This, together with the SNR’s evolutionary state and location in a complex region of the Galaxy, leads us to believe that the supernova explosion was of **core-collapse type**, and the *ROSAT* source, **located close to source 1** in Figure 2, is possibly the collapsed core.

The small number of counts in the *ROSAT* data did not allow, however, for spectroscopy or detailed imaging of the overall region or point sources to be done, so an *XMM-Newton* observation, described in §2, has been carried out, primarily in order to make an X-ray detection of the SNR, and to study the *ROSAT* source.

Because the integration time was unfortunately significantly reduced by proton flaring (see §2), distinguishing diffuse X-ray emission from the SNR on the images was not possible, but we estimate the strength of its X-ray emission through spectral analysis. In this work, the main focus is to examine the discrete sources in the field. We were able to resolve a few dozen sources, **18 of which have more than 25 counts according to the source detection**, and extract spectra for eight of them, including two very close to the location of the *ROSAT* source, which we preliminarily consider to be the likely neutron star associated with G107.5–1.5.

## 2 OBSERVATION

The SNR G107.5–1.5 was observed with *XMM-Newton* in full window mode on 2007 January 23 for 34.8 ks (Obs ID: 0400600101) The pn (Strüder et al. 2001) and MOS (Turner

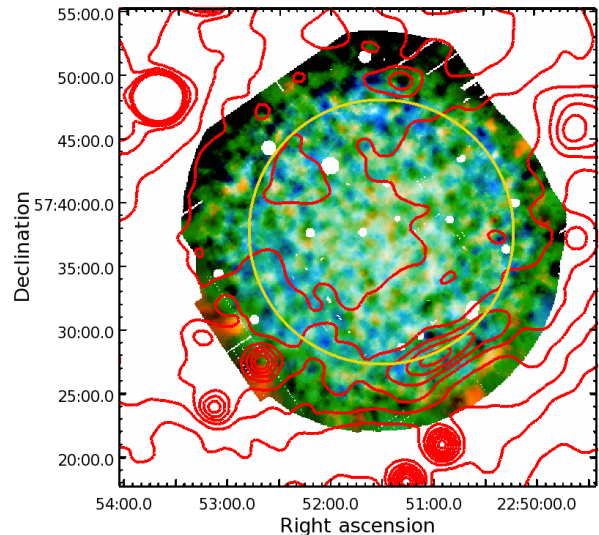


**Figure 1.** False colour *XMM-Newton* mosaic image of SNR G107.5–1.5. Sources have been excised and the image has been smoothed with a threshold of 50 counts. The orange component corresponds to 0.5–2.5 keV and the cyan component corresponds to 2.5–10 keV. The energy bands were chosen so that each of the component images has an approximately equal number of counts. The images have had particle and soft proton backgrounds subtracted and are exposure-corrected. The radio contours are overlaid in red. The extraction region used for the spectral analysis in §4.1 is shown in yellow. Coordinates are J2000.

et al. 2001) data were reduced with **Scientific Analysis System (SAS)**<sup>1</sup> version 13.5.1.

Images and spectra were extracted using the *XMM-Newton Extended Source Analysis Software (ESAS)* package (Snowden et al. 2004), which calls various SAS routines to filter out proton flaring, identify and remove point sources (for the diffuse analysis), and estimate backgrounds for the diffuse spectra by using the non-illuminated corners of the detectors. Because of the high amount of proton flaring, the integration time was reduced to 11.7 ks for pn, 15.7 ks for MOS1, and 15 ks for MOS2.

## 3 IMAGING

Figures 1 and 2 show the *XMM-Newton* X-ray mosaic images in the 0.5–10 keV range, with CGPS contours overlaid. These are combined, exposure-corrected images from pn, MOS1, and MOS2 data from which particle and soft proton backgrounds have been subtracted. Many discrete point-like sources and a few extended sources, most of which lie within the radio shell, can be seen on Figure 2.

Two methods were used to remove the contribution of the detected point sources (see §3.1 for a description of the source detection) to facilitate a close examination of the diffuse X-ray emission. For the first, the reconstructed image of the detected sources produced by the source detection program was subtracted from the original image. The second

<sup>1</sup> <http://xmm.esa.int/sas/>

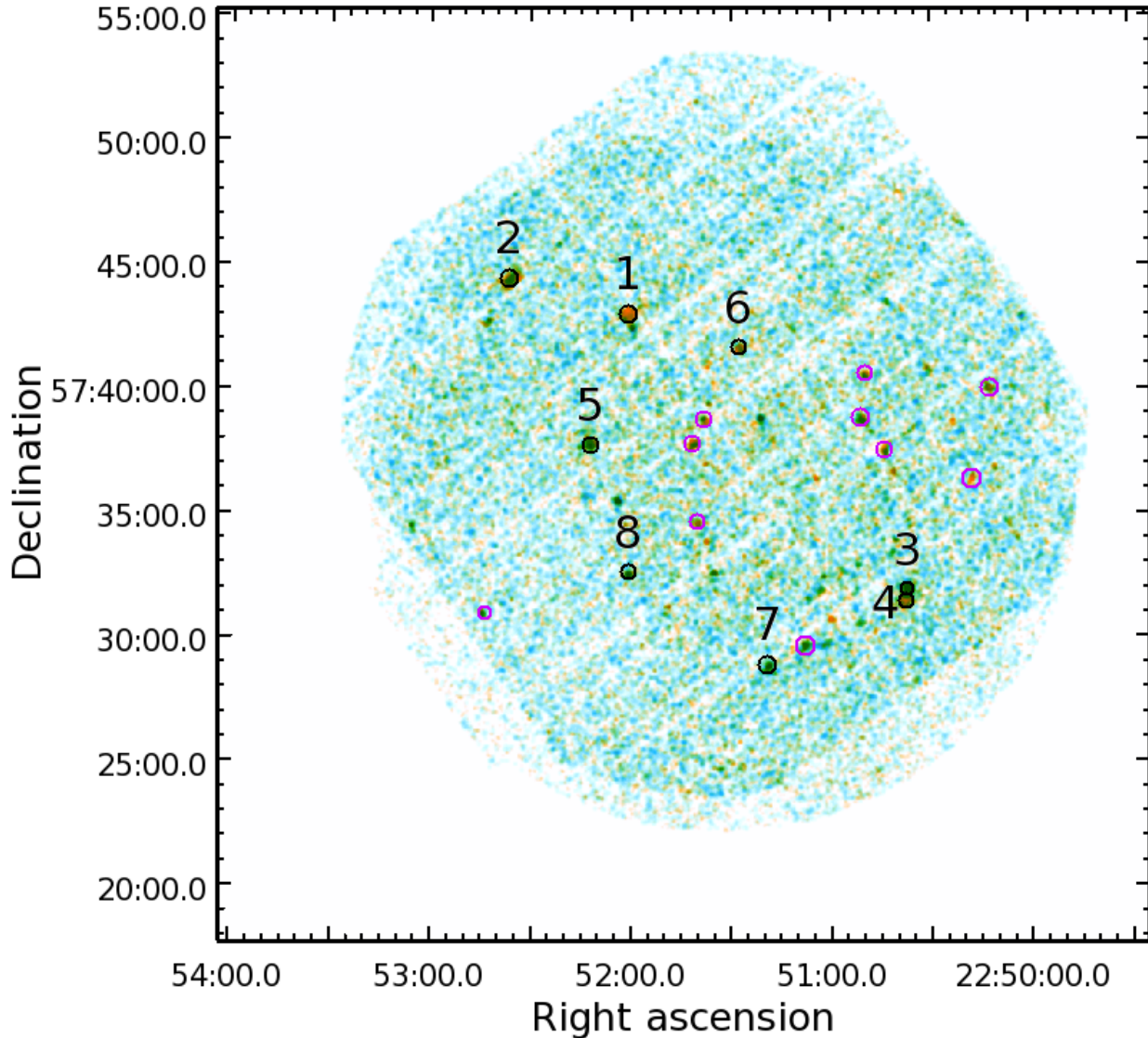


**Figure 2.** False colour *XMM-Newton* mosaic image of SNR G107.5–1.5. Energy bands, background subtraction, and exposure-correction are the same as in Figure 1. The image has been smoothed with a threshold of 20 counts. Detected point sources are circled, and those from which spectra could be extracted are numbered 1–8 and identified with black circles.

method is to exclude regions at the locations of the detected sources, which is done using the ESAS routine *cheese*.

Images generated using the above-mentioned methods show no discernible diffuse X-ray emission (see Figure 1). This is possibly because the exposure time was significantly shortened (by more than 50%) due to the proton flares during the observation. The objective of this paper is therefore to address the nature of the point sources, with specific focus on source 1, which is very near the location of the *ROSAT* source. However, an attempt has been made to identify areas of SNR X-ray emission through spectral analysis. This effort is described in § 4.1.

### 3.1 Source Detection

To identify the X-ray sources in the *XMM-Newton* observations (both point sources and extended sources) in the

SNR G107.5–1.5 field, *ewavelet*, a wavelet detection algorithm which is part of the SAS package, was used. For each source, the output of the routine gives the position on the image, source counts, and source extent (FWHM), as well as errors in those quantities. The program also produces a reconstructed image of the detected sources, which can be subtracted from the original image to reveal any diffuse emission, as described in the previous section. Point sources are identified by choosing sources at all wavelet scales with a significance of greater than  $3\sigma$  and a less than 5 pixel extent (FWHM), which corresponds to about 17 arcseconds, on the combined 0.5–2.5 keV and 2.5–10 keV images. This conservative requirement is based on the fact that off-axis sources have a larger PSF than those toward the centre of the images. This effect is more pronounced at higher energies, and the 5 pixel extent limit corresponds to the approximate PSF of a source at the highest energy at the edge of the field

of view. The 18 sources with more than 25 counts from the source detection are shown in Figure 2 as **magenta** or black circles. Only source 3 was significantly detected on both the soft and hard images. The other sources were detected only in the soft-band image, with no detection or a detection of fewer than 25 counts on the hard image. Source detection performed on the individual pn, MOS1, and MOS2 images in those energy ranges yielded similar source lists. The 2XMMi catalogue (Watson et al. 2009) contains the 18 sources described above, as well as 43 fainter point sources within the region covered by the observation.

Eight of the eighteen point sources indicated on Figure 2 are sufficiently bright to have spectra of more than 100 counts extracted, and these are indicated as the numbered sources in Figure 2. Table 1 lists these sources with their **coordinates and positional errors**. Source 1, which is near the centre of the radio shell, has coordinates  $\alpha(\text{J2000}) = 22\text{h } 52\text{m } 00\text{s}.629$ ,  $\delta(\text{J2000}) = 57^\circ 42' 59''.00$ , with a positional error of  $0''.5$ , and is coincident with the unidentified *ROSAT* source 1RXS J225203.8+574249 and is furthermore identified as 2XMMi J225200.3+574259 (see Table 1).

Figure 2 shows a false-colour image of the sources. Orange corresponds to 0.5–2.5 keV and cyan corresponds to 2.5–10 keV. **This image provides a rough indication of the spectral hardness of the sources.** Table 1 includes a column giving the total counts in the spectrum for each source. Sources 1, 2, 4, and 6 appear softer than the others on the image. Sources 3 and 4, though very close to each other, were detected as two distinct point sources, and **they clearly have different hardnesses.**

The *Vizier* tool (Ochsenbein et al. 2000) was used to search for optical and infrared counterparts to the X-ray sources. The optical/X-ray flux ratio has been calculated for each counterpart candidate, which is meaningful and accurate only if the counterpart candidate is the true counterpart, and is the only (or at least the brightest) X-ray source within the extraction circle. As can be seen from Table 2, sources 3, 7, and 8 have no close optical counterpart candidate.

The blue magnitude is converted into optical flux with the relation  $F_1 = F_2 \cdot 10^{(m_2 - m_1)/2.5}$  and compared with the X-ray flux (obtained from the spectral fitting, described below), and this ratio is one factor that can be checked to favour identification as a neutron star. In the above equation,  $m_1$  and  $m_2$  are the blue magnitudes of the object and a standard star, respectively, and  $F_1$  and  $F_2$  are their fluxes. Typical neutron stars have a flux ratio in optical to X-ray bands of  $\sim 1 - 10$  (Lyne & Graham-Smith 1998), whereas stars have a minimum flux ratio of  $10^3$  (Testa 2010). X-ray emitting O- or B-type stars such as  $\eta$  Carinae (Corcoran et al. 2000) or  $\tau$  Scorpii (Mewe et al. 2003) have a ratio of  $\sim 10^7$  (this calculation is confirmed in Nazé et al. 2011, by means of the use of bolometric optical fluxes).

## 4 SPECTROSCOPY

### 4.1 Diffuse emission

To estimate the diffuse flux from the SNR, spectra were extracted from a single circular region with a radius of 10 arcminutes centered at  $\text{RA} = 22\text{h}51\text{m}30.4\text{s}$ ,  $\delta = 57^\circ 37' 46''$

in pn and MOS data. **Regions surrounding detected sources were excluded from the extraction.** In addition, a *ROSAT* All-Sky Survey (RASS) spectrum from a 1–2 degree annulus was retrieved from the HEASARC X-ray background tool v2.5<sup>2</sup>, and all four spectra were used for the fits.

Following the ESAS cookbook<sup>3</sup>, a model comprising instrumental Gaussian lines, three thermal components corresponding to the local hot bubble and hotter and cooler galactic halo, and a power law representing the background of unresolved X-ray sources, was preliminarily constructed using XSPEC<sup>4</sup> version 12.8. The non-instrumental background components were considered to have fixed parameters across the entire region, and an additional broken power law component that was not folded through the instrumental response was used to fit the soft proton background. This final component was given a break energy of 3.0 keV, and the photon indices for the two MOS instruments were tied together. In the pn spectra, the soft proton background was found to be negligible and was removed from the fit. The thermal components were modelled with the Astrophysical Plasma Emission Code (APEC) model (Smith et al. 2001), modified (if necessary) by Wisconsin absorption (*wabs* in XSPEC; Morrison & McCammon 1983).

In the model described above, the thermal component corresponding to emission from the local hot bubble is unabsorbed and has a temperature of  $kT \sim 0.1$ . Both components representing the halo emission are absorbed with an  $N_{\text{H}}$  value in the direction of the SNR found from both the HEASARC Column Density tool<sup>5</sup> and the *Colden* tool on the *Chandra* website<sup>6</sup> to be  $\sim 6 \times 10^{21} \text{ cm}^{-2}$  from Galactic maps (Kalberia et al. 2005; Dickey & Lockman 1990; Stark et al. 1992).

Because the line of sight is so close to the galactic plane, the component representing the hotter galactic halo emission includes thermal contribution from the galactic disk. This means that the absorption coefficient for the component varies over the emitting region, and it must be considered that the average absorption coefficient (that which will produce the best fit for the model) may not be as great as the value listed above because some of the emission arises from regions interior to the galaxy.

Unfortunately, the temperatures of the Galactic (halo and disk) emission and the SNR emission are expected to be similar ( $\sim 0.25 - 0.7$  keV for the Galactic emission and  $\sim 0.5$  keV for the SNR emission). In addition, the hydrogen column density,  $N_{\text{H}}$ , in the direction of the SNR, has been determined to be in a range of  $0.1$  to  $0.6 \times 10^{22} \text{ cm}^{-2}$ . The lower limit on  $N_{\text{H}}$  was determined from radio data which included only neutral atomic hydrogen (Kothes 2003), and the upper value was determined from measurements of the absorption along the full line of sight through the galaxy as above. The upper value is also consistent, within error, with the radio determination. Because the temperatures and

<sup>2</sup> <http://heasarc.gsfc.nasa.gov/cgi-bin/Tools/xraybg/xraybg.pl>

<sup>3</sup> <ftp://xmm.esac.esa.int/pub/xmm-esas/xmm-esas.pdf>

<sup>4</sup> <http://heasarc.gsfc.nasa.gov/xanadu/xspec/>

<sup>5</sup> <http://heasarc.gsfc.nasa.gov/cgi-bin/Tools/w3nh/w3nh.pl>

<sup>6</sup> <http://cxc.harvard.edu/toolkit/colden.jsp>

**Table 1.** Catalogue of X-ray sources detected inside SNR G107.5–1.5, with corresponding 2XMMi name (Watson et al. 2009). The positional error is  $1\sigma$  and corresponds to that found in the 2XMMi catalogue. The coordinates quoted for this paper give the locations of the centroids of the extraction circles for the point sources.

#	IAU Name 2XMMi	This paper		2XMMi catalogue		Pos. Err. (arcsec)	Spectral counts	Hardness ratio <sup>a</sup>
		$\alpha_{J2000.0}$	$\delta_{J2000.0}$	$\alpha_{J2000.0}$	$\delta_{J2000.0}$			
1	J225200.3+574259	22 52 00.63	57 42 59.0	22 52 00.41	57 42 59.0	0.5	667	-1
2	J225236.3+574422	22 52 36.58	57 44 21.7	22 52 36.31	57 44 22.2	0.6	714	-0.71
3	J225036.9+573154	22 50 37.05	57 31 53.3	22 50 36.94	57 31 54.5	0.6	256	-0.28
4	J225037.9+573127	22 50 38.01	57 31 27.4	22 50 37.97	57 31 27.1	0.6	456	-1
5	J225212.1+573744	22 52 12.25	57 37 43.8	22 52 12.19	57 37 44.8	0.6	398	-0.21
6	J225127.4+574136	22 51 27.54	57 41 36.5	22 51 27.43	57 41 36.2	0.8	192	-1
7	J225118.7+572848	22 51 19.02	57 28 51.4	22 51 18.79	57 28 48.4	0.9	103	-0.09
8	J225200.9+573230	22 52 00.87	57 32 30.7	22 52 00.96	57 32 30.8	0.9	106	-0.32

<sup>a</sup> The hardness ratio is calculated from the counts derived from the source detection on the soft and hard images and is calculated as (H-S)/(S+H).

**Table 2.** List of optical (O) and infrared (I) counterpart candidates for each numbered X-ray source. Only those counterpart candidates within the X-ray error circle are listed. All counterpart candidate designations are from the USNO-B1.0 catalogue (Monet et al. 2003) or from the 2MASS catalogue (Skrutskie et al. 2006). **The B (the B1 magnitude is listed in this table) and J magnitudes correspond to those found in the USNO-B1.0 and 2MASS catalogues, respectively.**

Source #	Counterpart #	USNO-B1.0/2MASS name	Offset (arcsec)	B/J magnitude	$\frac{\text{Optical}}{\text{X-ray}}$ flux ratio <sup>a</sup>
1	O1	1477-0514019	3.6	9.4	4
	I1	22520056+5743004	1.5	6.1	
2	O1	1477-0514478	2.9	15.5	2
	O2	1477-0514481	2.1	14.9	
	I1	22523638+5744221	1.6	12.1	
4	O1	1475-0504764	0.63	11.8	3
	I1	22503796+5731271	0.4	9.9	
5	O1	1476-0513879	0.68	18.0	2
	I1	22521215+5737435	0.8	12.9	
6	O1	1476-0513126	0.74	15.7	4
	I1	22512749+5741359	0.7	12.1	
8	I1	22520093+5732294	1.4	17.1	

<sup>a</sup> The (logarithmic) optical to X-ray flux ratio is calculated assuming that only the single optical counterpart contributes to the X-ray flux. **The visible flux was calculated by using the fact that the B1 magnitude of Sirius is -0.09 (Monet et al. 2003) and the visible flux is  $1.1 \times 10^{-4}$  erg cm<sup>-2</sup> s<sup>-1</sup> (Liebert et al. 2005; Perryman 1997; Ochsenbein et al. 2000). An uncertainty of  $\sim 1$  on these values can be assumed.**

absorption coefficients of the two components are potentially indistinguishable, because the SNR emission is not discernible on the images, and because the spectral fitting did not allow for two separate components, the Galactic emission and the SNR emission have been combined into a single model component with a hydrogen column density up to  $6 \times 10^{21}$  cm<sup>-2</sup>, and the maximum flux of this component can be considered to be the upper limit on the SNR emission.

The final model therefore includes instrumental lines, broken power law components representing the soft proton

contamination in the MOS1 and MOS2 spectra, a power law representing the cosmic X-ray background and unresolved X-ray point sources, an unabsorbed thermal component, and two absorbed thermal components (“cool” and “warm”) corresponding to emission from the Galactic halo and disk and from the SNR. The higher temperature (warm) thermal component is likely to include all emission from the SNR.

The model was fit from 0.1 to 2.0 keV for *ROSAT*, from 0.4 to 10 keV for MOS1 and MOS2, and from 0.5 to 10 keV for pn to the model described above. The coefficients describing the hydrogen column density were fixed at  $6 \times 10^{21}$  cm<sup>-2</sup>

**Table 3.** Fit parameters pertaining to the cool and warm thermal components in the model described in §4.1 to which spectra extracted from the yellow circle in Figure 1 have been fitted. Errors are  $2\sigma$  uncertainties.

Component	$kT$ (keV)	0.5–5.0 keV Flux ( $10^{-12}\text{erg cm}^{-2}\text{s}^{-1}$ )	
		Absorbed	Unabsorbed
Cool	$0.15^{+0.02}_{-0.01}$	$(0.4 \pm 0.2)$	$(18 \pm 7)$
Warm	$0.58^{+0.04}_{-0.07}$	$(0.6 \pm 0.1)$	$(3.5 \pm 0.6)$

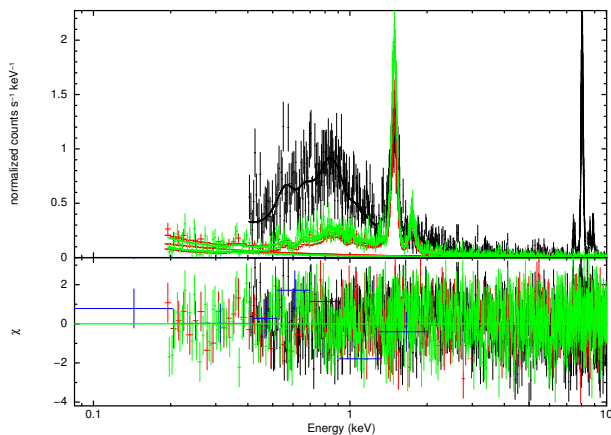


**Figure 3.** Fit of spectra extracted from the yellow circle in Figure 1 to the model described in §4.1. Black, red, green, and blue correspond to pn, MOS1, MOS2, and RASS spectra, respectively. The lower panel shows the deviation of the data from the model in terms of  $\chi$ .

to better constrain the fits. The fit was of reasonable quality, with  $\chi^2_\nu = 1.05$ . **The relevant parameters from the fit for the cool and warm thermal components are given in Table 3. Given the size of the extraction region and the unabsorbed flux of the warm thermal component,** this indicates an unabsorbed surface brightness upper limit for the SNR of  $\sim 2 \times 10^{30}$  erg arcmin $^{-2}$  s $^{-1}$ .

#### 4.2 Point sources

For each numbered source in Figure 2, spectra have been extracted from the pn and MOS data. The spectra have been grouped into bins containing at least 20 counts for pn and 10 counts for MOS. The background spectrum for each source has been extracted from an annulus surrounding the source, avoiding other nearby sources. The pn and MOS spectra for each individual object have been simultaneously fitted to an absorbed blackbody and/or an absorbed power law model. A likely identification for a Galactic X-ray point source with an infrared or optical counterpart is a coronally active late-type star (Warwick et al. 2011), so it is necessary to investigate each source with that possibility in mind. Thus, each source has also been fitted to an APEC model modified by Wisconsin absorption, with the expectation that coronal emitters will have a temperature  $kT$  of 0.1–1 keV (Güdel 2004). The results are shown in Tables 4, 5, and 6 for those sources whose spectra are well fitted with

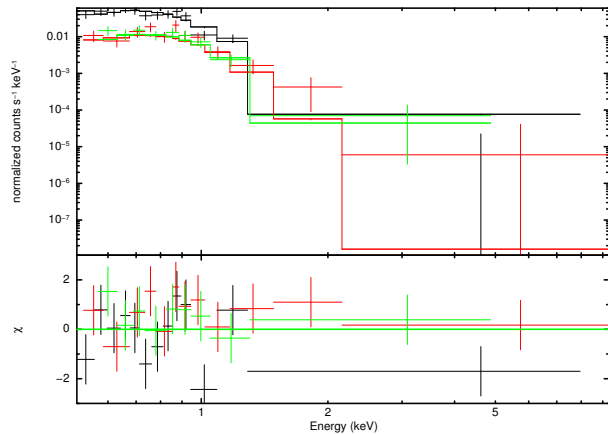


**Figure 4.** Spectrum of source 1 fit to an absorbed blackbody. The fitted parameters are given in Table 4. Black, red, and green correspond to pn, MOS1, and MOS2 spectra, respectively. The lower panel shows the deviation of the data from the model in terms of  $\chi$ .

these models, and Figure 4 shows the fit of the spectrum of source 1 to an absorbed blackbody.

As was done with the diffuse spectrum, as described in § 4.1, the  $N_H$  was estimated to be  $0.6 \times 10^{22}$  cm $^{-2}$  for sources associated with the SNR, and for some of the blackbody and power law fits, the value of  $N_H$  was frozen at this value. This was done in order to better constrain the fits, and to determine the spectral parameters for each source, assuming an association with the SNR exists. Some spectra were not fitted well with the absorption parameter frozen in this way, and those are not shown in the tables.

When the  $N_H$  value was set to  $0.6 \times 10^{22}$  cm $^{-2}$ , the value of  $\chi^2_\nu$  was greater than 2 for sources 5 and 6 for the absorbed blackbody fit, and source 5 for the absorbed power law fit, which indicates an unsatisfactory fit, but it is a possible value of  $N_H$  for the rest of the sources. The error bars on the parameters are unfortunately very large for many of the sources, leading to large uncertainties in the flux values. It is unclear for many of the sources which of the models, blackbody, APEC, or power law, is the best fit.

For the objects fitted with an absorbed blackbody model, the emitting radii can be determined, given the approximate distance of 1.1 kpc. The radii are given in the rightmost column of Table 4 and those for sources 1, 2, and 4 are close to typical neutron star radii.

For many of the sources, the fit to an absorbed APEC is of comparable quality with the fit to an absorbed power law or blackbody, indicating that neither the neutron star nor the coronal emission explanation can be ruled out. For the absorbed APEC fit, sources 3 and 5 have unphysical  $kT$  values ( $> 9$  and  $> 18$  keV) and source 6 gives an unsatisfactory fit. For the absorbed blackbody or power law fits for the sources for which coronal emission can be ruled out, source 5 has an  $N_H$  value too low to be associated with the remnant, and this is also true for the blackbody fit for source 6. Source 6 is well fitted with a power law at the distance of the remnant. However, the power law index of  $5.9 \pm 0.9$  is very steep, ruling source 6 out as a neutron star candidate.

**Table 4.** Fit of discrete source spectra to an absorbed blackbody. Parameters are listed only where a satisfactory fit could be obtained. Errors are  $2\sigma$  uncertainties.

#	$N_H$ ( $10^{22}\text{cm}^{-2}$ )	$kT$ (keV)	0.5–5 keV Flux <sup>a</sup> ( $10^{-12}\text{erg cm}^{-2}\text{s}^{-1}$ )	$\chi^2_\nu$ ( $\nu$ )	Radius(km)
1	$0.3 \pm 0.2$	$0.10^{+0.03}_{-0.01}$	$0.3^{+1.5}_{-0.2}$	1.06 (31)	$20^{+5}_{-4}$
	(0.6) <sup>b</sup>	$0.082 \pm 0.004$	$2.1^{+0.7}_{-0.5}$	1.18 (32)	
2	$0.3 \pm 0.2$	$0.10 \pm 0.03$	$0.3^{+2.0}_{-0.2}$	1.12 (28)	$19^{+5}_{-4}$
	(0.6)	$0.083 \pm 0.004$	$2.1^{+0.5}_{-0.4}$	1.24 (29)	
3	$< 0.14$	$1.0^{+0.2}_{-0.1}$	$0.09^{+0.03}_{-0.02}$	0.81 (20)	$0.016^{+0.006}_{-0.005}$
	(0.6)	$0.9 \pm 0.1$	$0.11 \pm 0.02$	1.33 (21)	
4	$1.8^{+0.8}_{-0.7}$	$0.05 \pm 0.01$	(unconstrained)	0.76 (18)	$11^{+5}_{-3}$
	(0.6)	$0.09 \pm 0.01$	$1.1^{+0.7}_{-0.2}$	1.23 (19)	
5	$< 0.03$	$0.9 \pm 0.1$	$0.09 \pm 0.02$	1.77(20)	
6	$< 0.24$	$0.26^{+0.06}_{-0.05}$	$0.016 \pm 0.003$	1.10 (6)	
7	$< 1.1$	$0.7 \pm 0.3$	$0.03^{+0.02}_{-0.01}$	0.37 (6)	$0.019^{+0.017}_{-0.008}$
	(0.6)	$0.6 \pm 0.2$	$0.03 \pm 0.01$	0.457 (7)	
8	$< 3.2$	$0.5^{+0.2}_{-0.3}$	$0.03^{+0.12}_{-0.01}$	0.41 (2)	$0.03^{+0.05}_{-0.01}$
	(0.6)	$0.4^{+0.2}_{-0.1}$	$0.04^{+0.02}_{-0.01}$	0.30 (3)	

<sup>a</sup> All flux values refer to unabsorbed flux.

<sup>b</sup> A number in parentheses indicates a frozen value for the fit.

**Table 5.** Fit of discrete source spectra to an absorbed APEC. Parameters are listed only where a satisfactory fit could be obtained. Errors are  $2\sigma$  uncertainties.

#	$N_H$ ( $10^{22}\text{cm}^{-2}$ )	$kT$ (keV)	0.5–5 keV Flux ( $10^{-12}\text{erg cm}^{-2}\text{s}^{-1}$ )	$\chi^2_\nu$ ( $\nu$ )
1	$0.61^{+0.07}_{-0.12}$	$0.15^{+0.03}_{-0.01}$	$3 \pm 2$	1.15 (31)
2	$0.62^{+0.07}_{-0.14}$	$0.15^{+0.04}_{-0.03}$	$3^{+3}_{-2}$	1.09 (28)
3	$0.4^{+0.4}_{-0.2}$	$> 9$	$0.11^{+0.02}_{-0.03}$	0.91 (20)
4	$< 0.09$	$0.69 \pm 0.08$	$0.036^{+0.008}_{-0.007}$	1.26 (18)
7	$< 2.4$	$> 0.9$	$0.04^{+0.12}_{-0.02}$	0.365 (6)
8	$< 3.8$	$1.0^{+6.0}_{-0.7}$	$0.2^{+1.8}_{-0.1}$	0.29 (2)

## 5 TIMING

Because the pn observation was done in full window mode, the timing resolution of 70 ms limits pulsar searches to frequencies below approximately 7 Hz, which would exclude all millisecond pulsars and many ordinary pulsars, but may identify slowly rotating magnetars known to have periods  $P \sim 2 - 12$  s. The maximum frequency is applicable only to pulsars with an approximately sinusoidal lightcurve (i.e. a single peak per rotation). Pulsars with lightcurves which have additional peaks or other features would likely not be found unless the frequency was much less than 3.6 Hz. A negative result in a timing search thus does not indicate with any certainty that there is no pulsar present.

While producing the events file, the SAS software showed a possible problem with the timing for quadrant 3, involving jumps in the course timing parameter. This means

that the timing for sources 3 and 4 may not have been reliable, and there is no way to fix the timing with the data from this observation. Timing data from the other numbered sources would not have been affected by this.

Blind (i.e. the frequency is not known beforehand) timing searches were performed on the point sources of interest, including sources 3 and 4. For these searches, an FFT is first calculated, and then frequencies surrounding any significant peaks are searched using Rayleigh (Leahy, Elsner, & Weiskopf 1983) (also known as  $Z_1^2$ ),  $Z_2^2$ ,  $Z_3^2$  (Buccheri et al. 1983), and epoch folding tests. Only searches for frequencies of less than 1.8 Hz would have a sufficient number of bins per cycle (8) to reliably perform most of the tests.

**None of the point sources surrounding SNR G107.5–1.5 showed evidence of detectable pulsations.**

**Table 6.** Fit of discrete source spectra to an absorbed power law. Parameters are listed only where a satisfactory fit could be obtained. Errors are  $2\sigma$  uncertainties.

#	$N_{\text{H}}$ ( $10^{22}\text{cm}^{-2}$ )	$\Gamma$	0.5–5 keV Flux <sup>a</sup> ( $10^{-12}\text{erg cm}^{-2}\text{s}^{-1}$ )	$\chi^2_{\nu}$ ( $\nu$ )
3	< 0.64	$1.0^{+0.5}_{-0.4}$	$0.10^{+0.10}_{-0.03}$	0.87 (21)
	(0.6) <sup>b</sup>	$1.4 \pm 0.3$	$0.13 \pm 0.03$	0.94 (21)
5	< 0.1	$1.0 \pm 0.2$	$0.09^{+0.03}_{-0.01}$	0.97 (20)
6	< 0.71	$3^{+4}_{-1}$	$0.03^{+0.1}_{-0.01}$	1.06 (6)
	(0.6)	$5.9 \pm 0.9$	$0.27^{+0.05}_{-0.04}$	1.16 (7)
7	< 2.5	$2^{+3}_{-1}$	$0.06^{+0.9}_{-0.05}$	0.29 (6)
	(0.6)	$2.0^{+0.7}_{-0.6}$	$0.05^{+0.04}_{-0.02}$	0.27 (7)
8	< 5.4	> 2.9	$0.6^{+0.1}_{-0.4}$	0.46 (2)
	(0.6)	$3 \pm 1$	$0.07^{+0.05}_{-0.03}$	0.48 (3)

<sup>a</sup> All flux values refer to unabsorbed flux.

<sup>b</sup> A number in parentheses indicates a frozen value for the fit.

## 6 DISCUSSION

Because of their proximity to the centre of the radio shell, and because they can be fitted with an  $N_{\text{H}}$  value which conforms to the value for the SNR, sources 1 and 2 are of particular interest for the analysis presented in this paper. All other sources investigated in this study are also ruled out as neutron star candidates associated with this remnant, because of their proximity to the shell, their fitted value of  $N_{\text{H}}$ , and/or the lack of conformity between the individual spectra and both a power law and a blackbody.

Source 1 is a soft thermal source which is best fitted with an absorbed blackbody with a temperature of  $(9.5 \pm 0.5) \times 10^5$  K, when  $N_{\text{H}}$  is frozen at  $0.6 \times 10^{22} \text{ cm}^{-2}$ . Its corresponding luminosity, assuming a distance of 1.1 kpc, is  $(3.0^{+1.0}_{-0.7}) \times 10^{32} \text{ erg s}^{-1}$ . An absorbed power law fit to the spectrum of source 1 yields an unacceptably high value of  $\chi^2_{\nu}$ , indicating that its spectrum is dominated by a thermal component. These values are qualitatively comparable with the spectral parameters and luminosity of the Vela pulsar (Pavlov et al. 2001), and the age of 3–6 kyr is close to Vela’s characteristic age of 11 kyr, indicating that source 1 may be a Vela-like pulsar. Alternatively, this source could be a CCO candidate, since the X-ray spectra of CCOs are dominated by a thermal blackbody spectrum and have comparable luminosities (see e.g. Pavlov 2004). The spectral analysis did not rule out the possibility that the X-ray emission from source 1 arises from the corona of a late-type star, however, and since it is unlikely to find such a bright star by chance, this likely rules out Source 1 as a neutron star or CCO.

The fitted spectral parameters and proximity to the centre of the SNR radio shell of source 2 are similar to those of source 1, and it thus has similar merit as a neutron star candidate. Similarly, coronal emission is not ruled out as producing the X-ray emission from source 2, and since it does have a close optical and infrared counterpart, it is also likely ruled out as a neutron star or CCO.

Source 1 appears in the *ROSAT* All-Sky Survey catalogue, but source 2 does not. Since source 2 has a flux similar to that of source 1, according to the present X-

ray data, it is possible that it fell just short of inclusion in the RASS. Sources 1 and 2 are included in the *XMM-Newton* serendipitous source catalogue (Watson et al. 2009) as 2XMMi J225200.3+574259 and J225236.3+574422, respectively.

A deeper observation with higher angular resolution, such as with *Chandra*, would better allow closely-spaced X-ray sources to be distinguished, and would permit further spectroscopic study of the individual sources, particularly those that are too faint to have been studied in this paper. With more spectroscopic counts, multicomponent models could be used for the sources that do not fit well to simpler models, and source identification would be facilitated. In addition, with smaller X-ray error circles, association of X-ray sources with possible optical counterparts, such as that of source 1 with the nearby bright optical source, could be determined less ambiguously.

Timing observations for the as yet unidentified sources are also needed, and due to their proximity to each other, it would be possible to make a single *XMM-Newton* observation in small window mode which would include both sources and provide the timing resolution necessary for a pulsar search.

For X-ray detection of the diffuse emission from the SNR, a deeper *XMM-Newton* observation near the center of the radio shell and including many of the point sources (indicated with magenta circles on Figure 2) for which spectral analysis was not possible with the available data, would be best. It is possible that, without the reduction in integration time caused by the proton flaring, diffuse X-ray emission from the SNR would have been detected, so another *XMM-Newton* observation of the same duration or longer would be beneficial for a greater understanding of this low-surface brightness, highly polarized SNR.

## 7 ACKNOWLEDGMENTS

*XMM-Newton* is an ESA science mission with instruments and contributions directly funded by ESA Member States



and NASA. This research was supported by Natural Sciences and Engineering Research Council of Canada (NSERC). SSH acknowledges support by NSERC, the Canadian Space Agency, Canada Foundation for Innovation, and the Canadian Institute for Theoretical Astrophysics. This research made use of NASA's Astrophysics Data System and the High Energy Astrophysics Science Archive Research Center (HEASARC). We would like to thank the anonymous referee for comments that helped to improve the paper.

## REFERENCES

- Buccheri, R., Bennet, K., Bignami, G. F., et al., *A&A*, 128, 245–251, 1983.
- Corcoran, M. F., Fredericks, A. C., Petre, R., Swank, J. H., Drake, S. A., *ApJ*, 545, 420–428, 2000.
- Dickey, J. & Lockman, F., *ARAAS*, 28, 215, 1990.
- Foster, T. J., Cooper, B., Reich, W., Kothes, R., West, J. *A&A*, 549, A107, 2013.
- Gotthelf, E. V., Halpern, J. P., AIP Conf. Proc. 983, 320–324, 2008.
- Güdel, M., *Astron & Astrophys. Rev* 12, 71–237, 2004.
- Jackson, M. S., Safi-Harb, S., Kothes, R., Foster, T., *ApJ*, 674, 936–953, 2008.
- Joye, W. A. & Mandel, E., Astronomical Data Analysis Software and Systems XII ASP Conference Series, 295, 489, 2003. H. E. Payne, R. I. Jedrzejewski, and R. N. Hook, eds.
- Kalberla P. et al. *A&A*, 440, 775, 2005.
- Kargaltsev, O. & Pavlov, G., IP Conference Proceedings, 983, 171–185, 2008.
- Kothes, R., Landecker, T. L., Foster, T., Leahy, D. A., *A&A*, 376, 641–649, 2000.
- Kothes, R., *A&A*, 408, 187–192, 2003.
- Kothes, R., Fedotov, K., Foster, T., Uyaniker, B., *A&A*, 457, 1081–1093, 2006.
- Leahy, D. A., Elsner, R. F., & Weisskopf, M. C., *ApJ*, 272, 256–258, 1983.
- Liebert, J., et al., *ApJ*, 630, L69–L72, 2005.
- Lyne, A. G., Graham-Smith, F. 1998, *Pulsar Astronomy*, Cambridge: Cambridge University Press.
- Mereghetti, S., Proceedings of the 26th Texas Symposium on Relativistic Astrophysics, Sao Paulo, December 16–20 2012 (<http://arxiv.org/abs/1304.4825>)
- Mewe, R., Raassen, A. J. J., Cassinelli, J. P., van der Hucht, K. A., Miller, N. A., Güdel, M., *A&A*, 398, 203–211, 2003.
- Monet, D. G., Levine, S. E., Canzian, B., et al., *AJ*, 125, 984–993, 2003
- Morrison, R., McCammon, D., *ApJ*, 270, 119–122, 1983
- Nazé, Y., et al. *ApJS*, 194, 7, 2011.
- Ochsenbein F., Bauer P., Marcout J., *A&AS*, 143, 23–32, 2000.
- Pavlov, G. G., Zavlin, V. E., Sanwal, D., Burwitz, V. , & Garmire, G. P. *ApJ*, 552, L129–L133, 2001.
- Pavlov, G. G. Young Neutron Stars and Their Environments, IAU Symposium no. 218, Eds. Fernando Camilo and Bryan M. Gaensler. San Francisco, CA: Astronomical Society of the Pacific, 239, 2004.
- Perryman M.A.C., ESA, 1997, The Hipparcos and Tycho catalogues, ESA SP-1200, ESA Publications, Noordwijk
- Skrutskie, M. F., et al. *ApJ*, 131, 1163–1183, 2006.
- Smith, R., Brickhouse, N., Liedhal, D., & Raymond, J., *ApJ*, 556, L91–L95, 2001.
- Snowden, S., Collier, M., & Kuntz, K. *ApJ*, 610, 1182, 2004.
- Strüder, L., Briel, U., Dennerl, K., et al., *A&A*, 365, L18–L26, 2001
- Stark, A. et al., *ApJ Suppl.* 79, 77, 1992
- Taylor, A. R., Gibson, S.J., Peracaula, M., et al., *AJ*, 125, 3145–3164, 2003.
- Testa, P., *Publications of the National Academy of Science*, 107 (16), 7158–7163, 2010.
- Tian, W. W., Leahy, D. A., Foster, T. J. *A&A*, 465, 907–911, 2007.
- Tsujimoto, T., Nomoto, K., Yoshii, Y., Hashimoto, M., Yanagida, S., & Thielemann, F.-K. *MNRAS*, 277, 945–958, 1995.
- Turner, M. J. L., Abbey, A., Arnaud, M., et al., *A&A*, 365, L27–L35, 2001.
- Vink, J., The Astronomy and Astrophysics Review 20, 1, 2012 see <http://adsabs.harvard.edu/abs/2012A%26ARv..20...49V>
- Warwick R. S., Pérez-Ramirez, D., & Byckling, K. *MNRAS*, 413, 595–610, 2011.
- Watson et al., *A&A*, 493, 339–373, 2009.